Spectroscopy for development of plasma sources for water window imaging

Gerry O'Sullivan, Goki Arai, Thanh-Hung Dinh, Padraig Dunne, Hiroyuki Hara, Paddy Hayden, Takeshi Higashiguchi, Yoshiki Kondo, Bowen Li, Luning Liu, Ragava Lokasani, Elaine Long, Deirdre Kilbane, Takanori Miyazaki, Hayato Ohashi, Fergal O'Reilly, Paul Sheridan, John Sheil, Emma Sokell, Atsushi Sunahara, Chihiro Suzuki, Yuhei Suzuki, Elgiva White and Tao Wu.

ISCA Japan International Strategic Cooperation Award

2015 Source Workshop, UCD 11th November 2015

Outline

Background:
Basics of laser produced plasmas, unresolved transition arrays.

Spectroscopy:
Δn=0 Unresolved Transition Arrays
Δn=1 Unresolved Transition Arrays

Future Plans and Conclusions

Water window

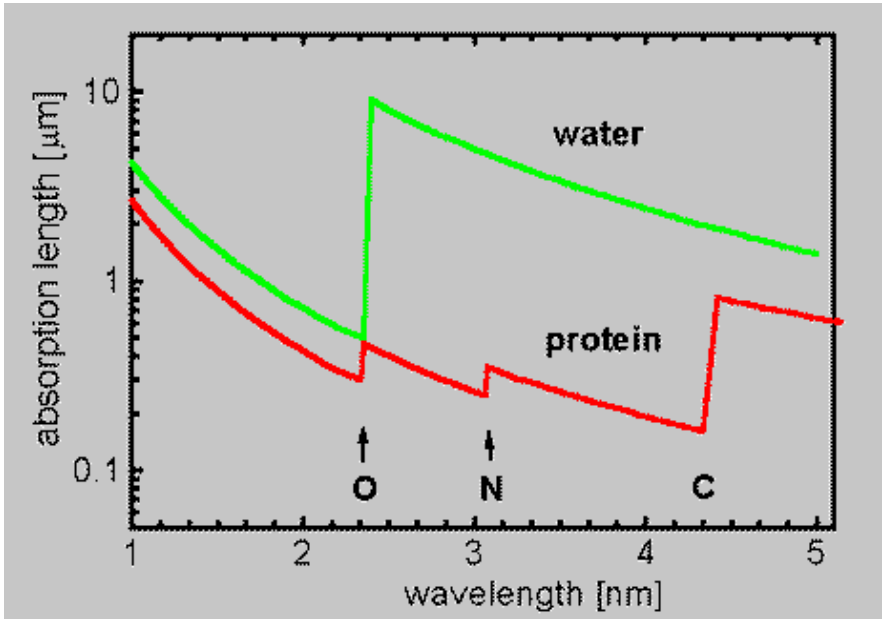

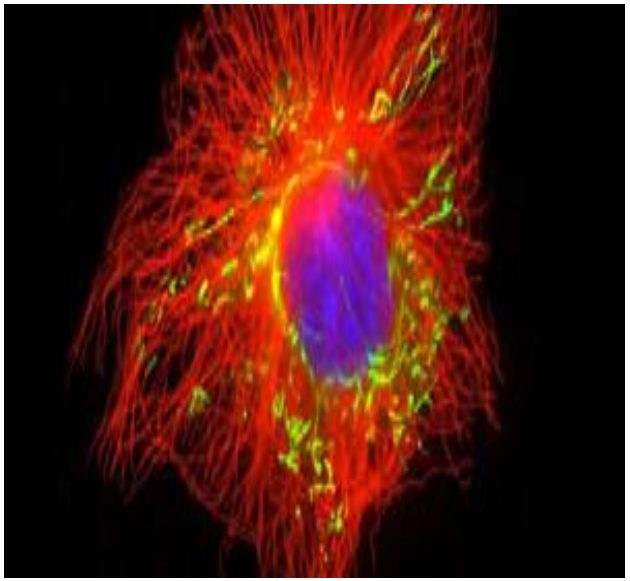

Water window : 2.34-4.38 nm.

Relative transparency of water allows investigation of biomolecules, cells and proteins in their natural aqueous environment by x-ray transmission microscopy or tomography

SXR Tomography: Zone Plate Optics

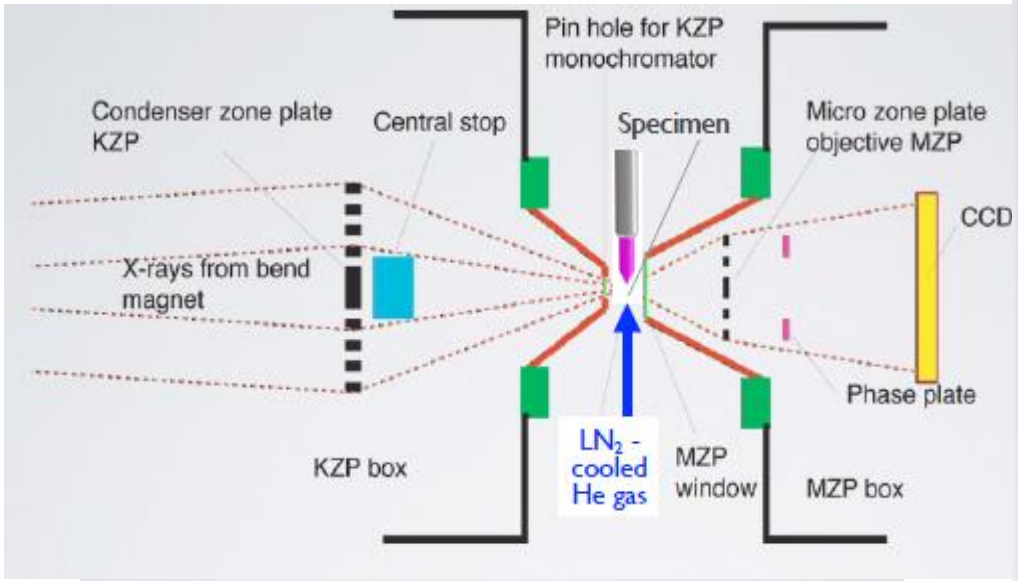

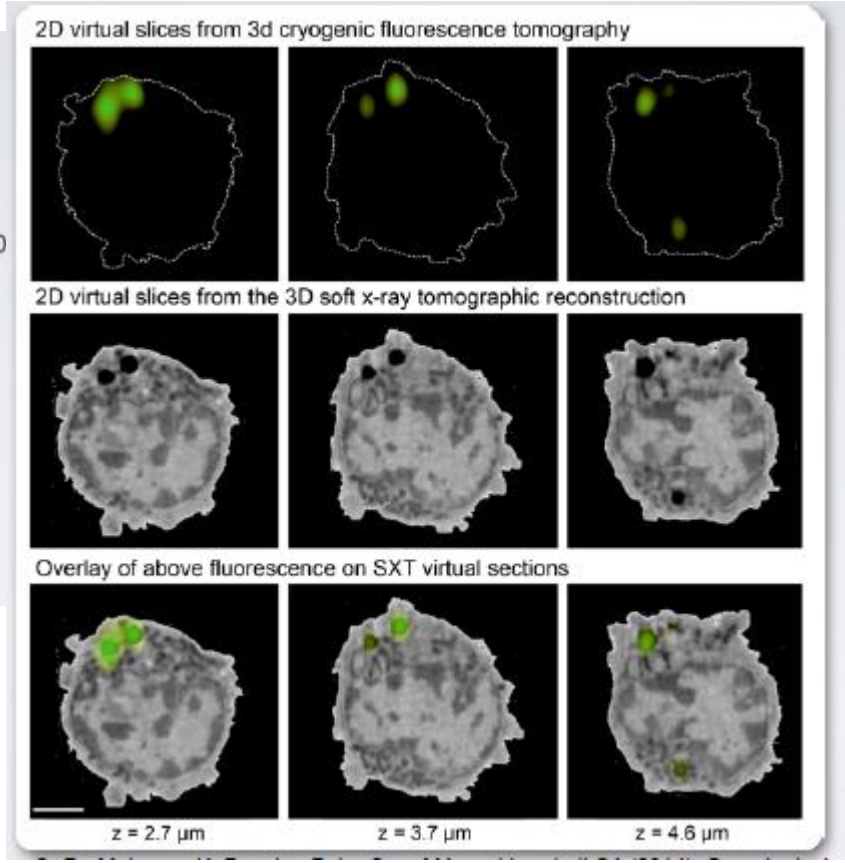

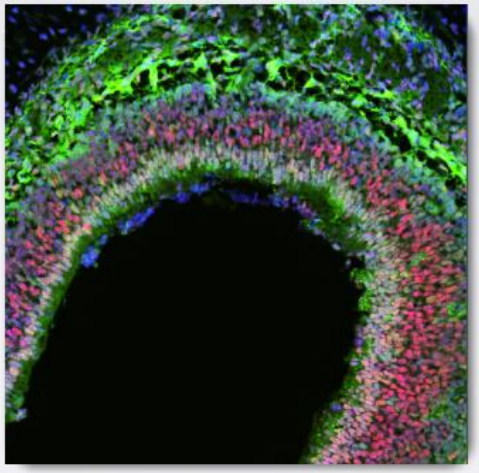

Stavros Lomvardas, UCSF

Smith EA, McDermott G, Do M, Leung K, Panning B, Le Gros MA and Larabell CA (2014). Quantitatively imaging chromosomes using correlated cryo-fluorescence and soft x-ray tomographies. *Biophysical Journal*. 107(8) 1988-96.

Carolyn Larabelle, EUV Source Workshop, UCD S-3 2014

Network for single shot water window imaging source development with reflective optics

Material	Wavelength (nm)	Reflectivity (%)
Cr/V	2.42	9
Cr/Ti	2.73	17
TiO_2/ZnO	2.74	29
Cr/Sc	3.12	32
Cr/Sc	3.14	21
Cr/Sc B_4C	3.15	32.1
Cr/Sc	3.35	10
Cr/Sc	3.37	5.5

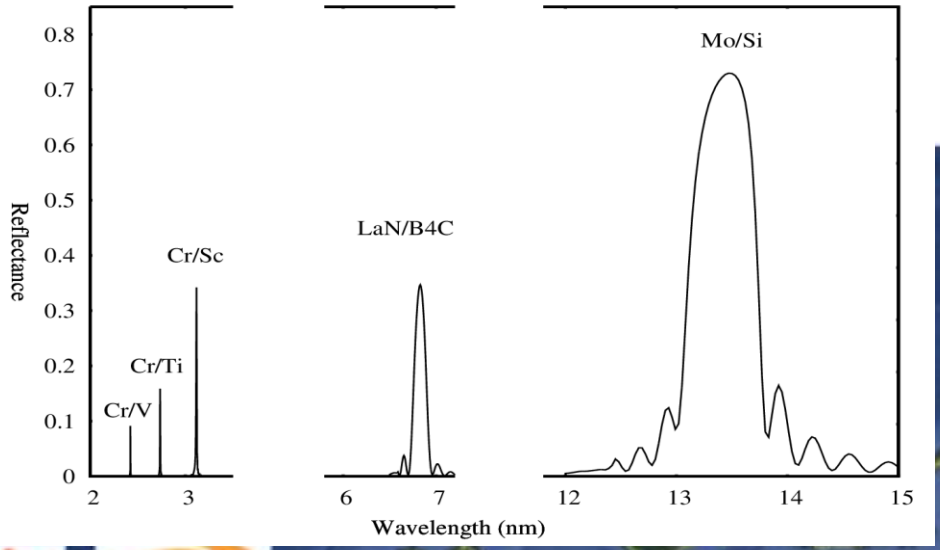

Laser produced plasmas (LPPs)

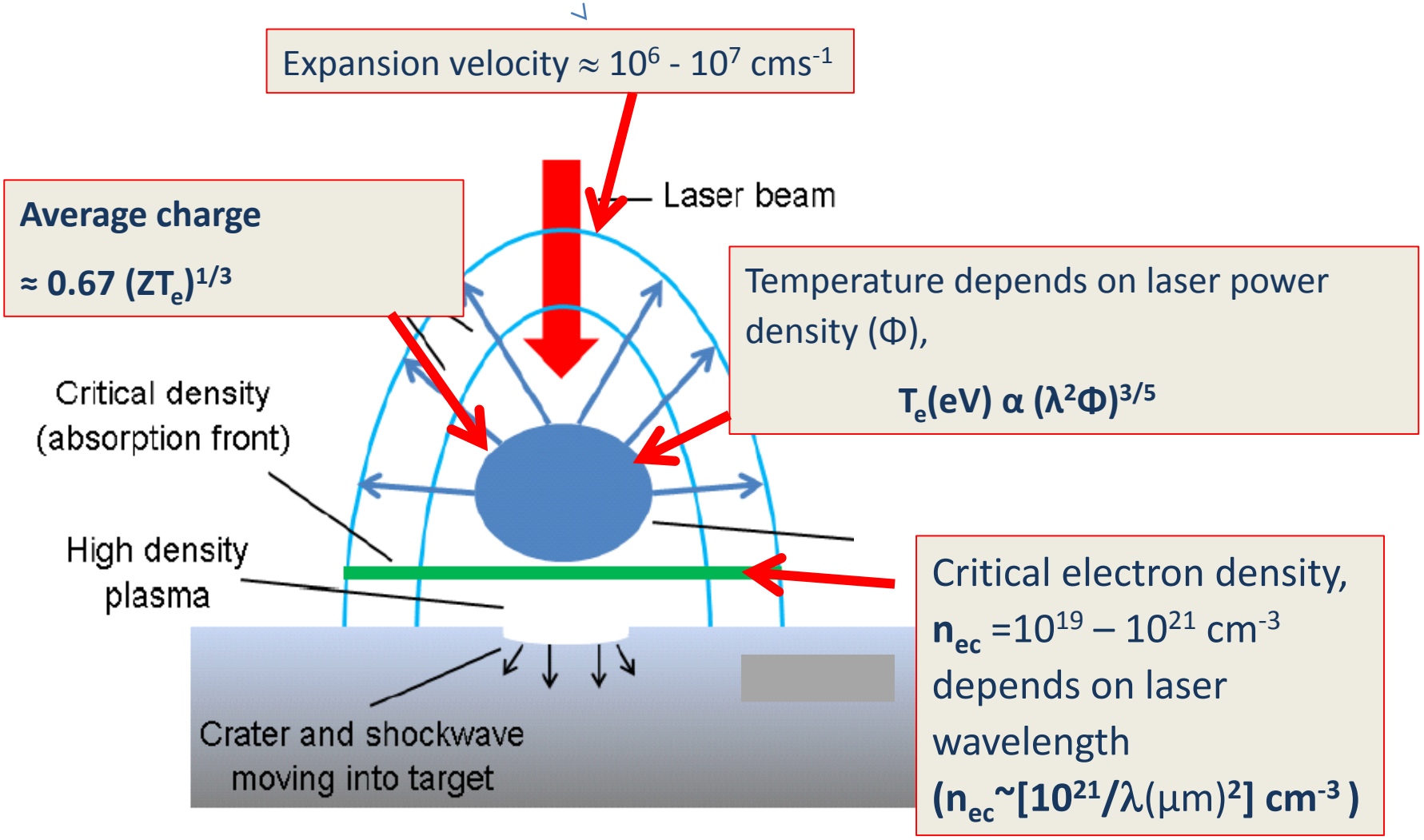

Comparison of water window emission spectra

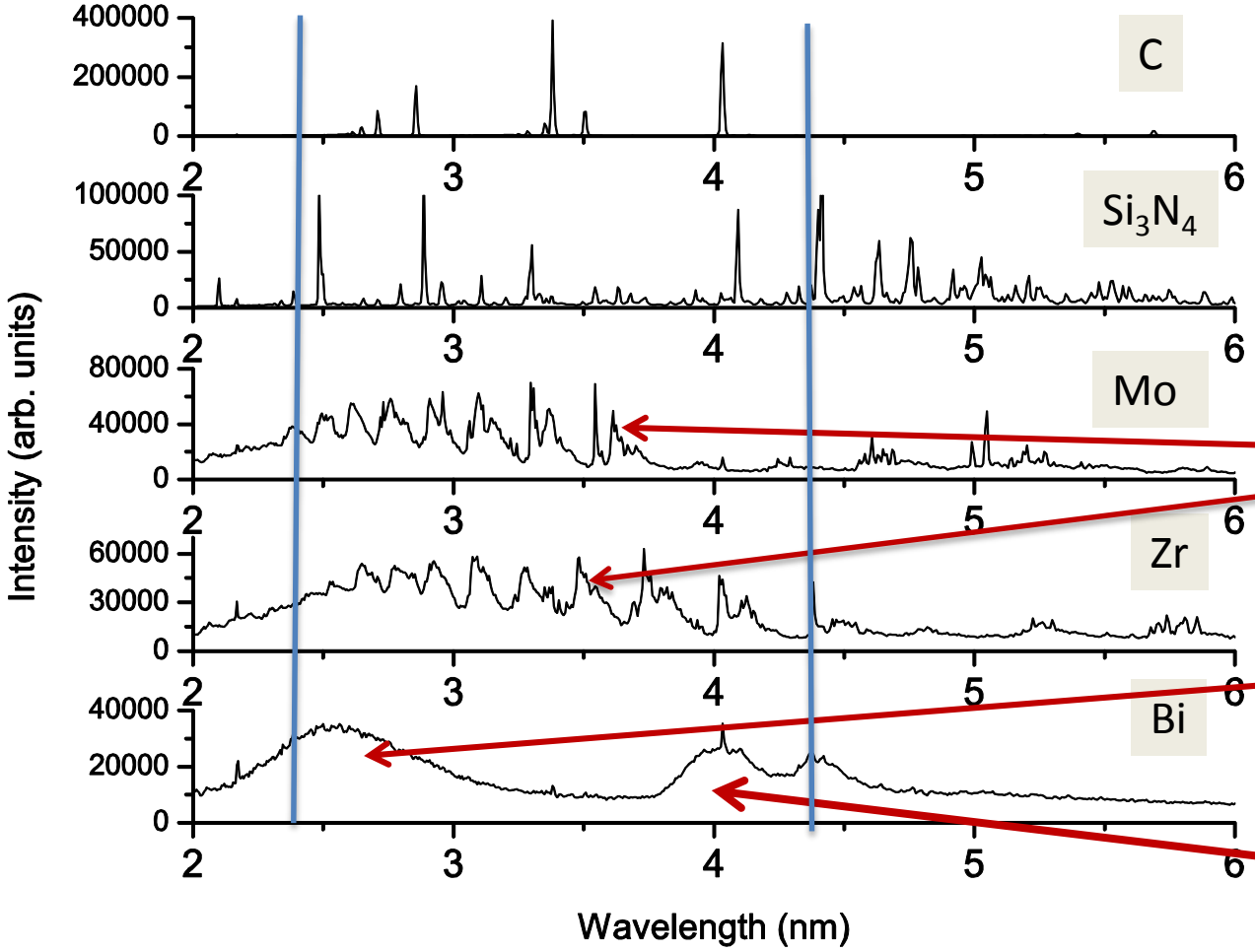

Δn = 1, 3d-4f Unresolved transition array (UTA)

Δn = 1, 4f-5g UTA

Δn = 0, 4d-4f & 4p-4d UTA

Time-integrated spectra from picosecond-laser-produced plasmas

SXR spectra studied

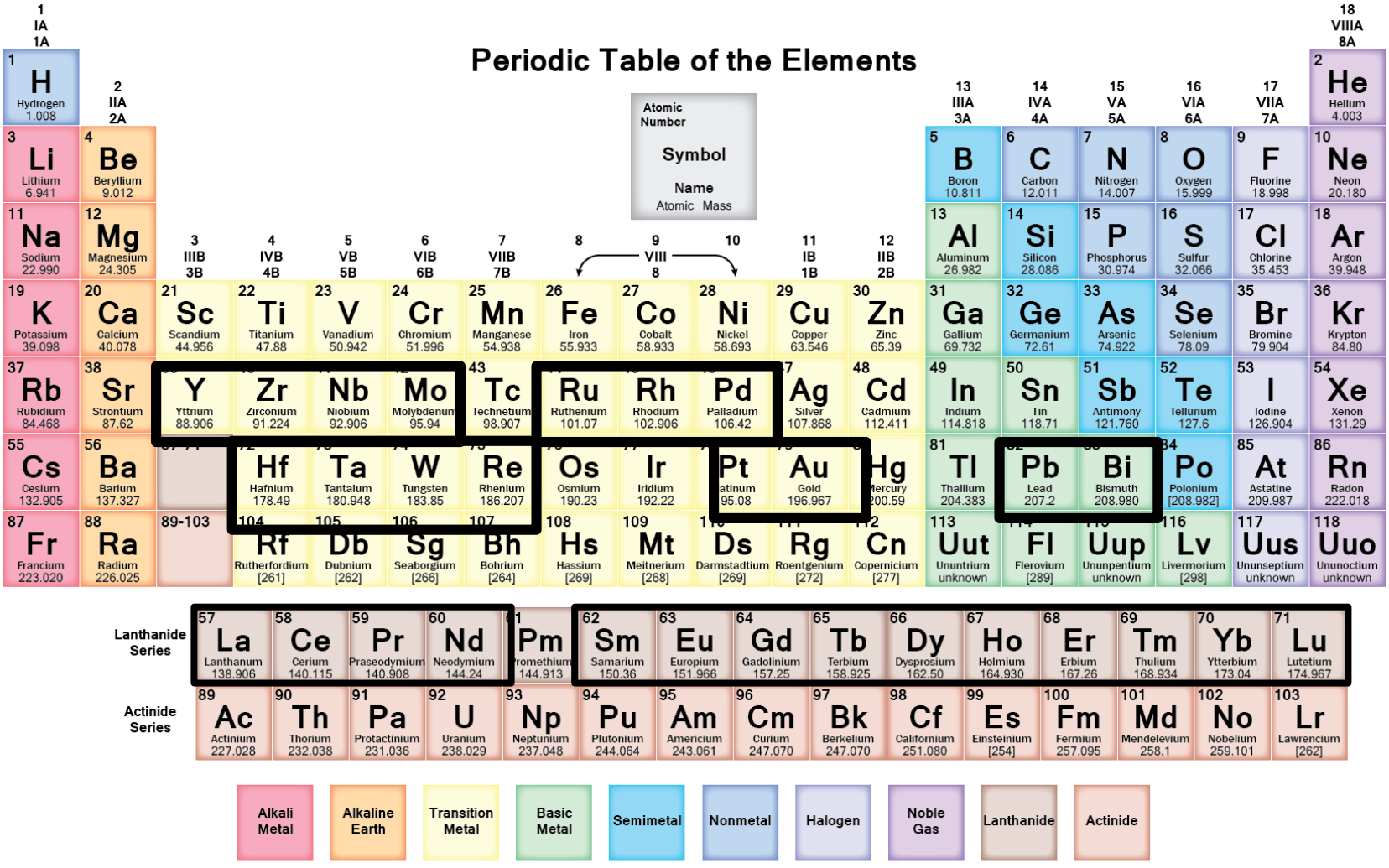

Two types of UTA in XUV spectra

Δn = 0

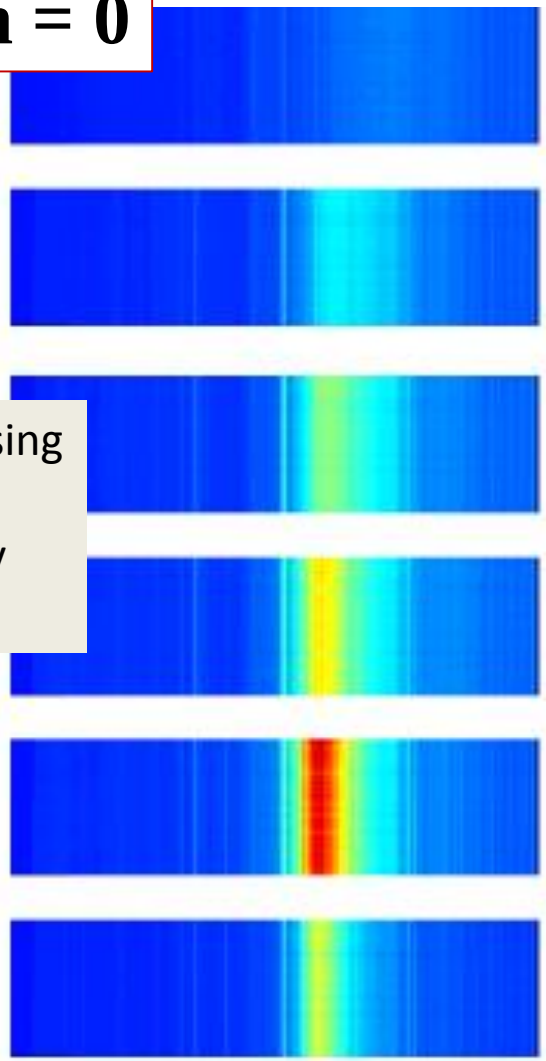

Increasing power density ↓

$4p^6 4d^{N+1} - 4p^6 4d^N 4f + 4p^5 4d^{N+2}$ in Sn

Δn > 0

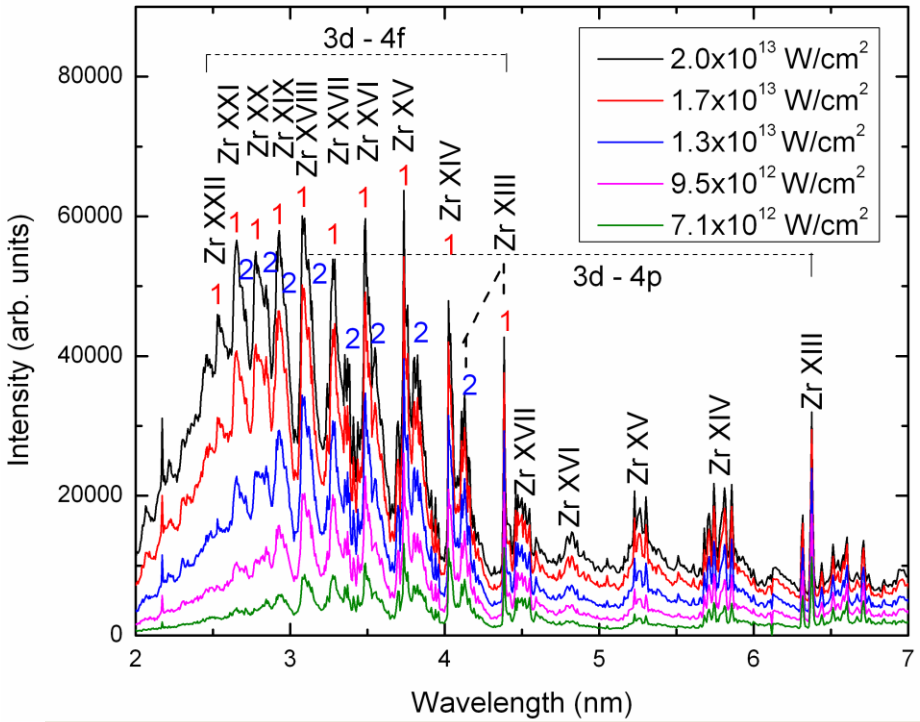

Δn = 0 transitions overlap in adjacent ion stages.

Δn = 0 transitions do not overlap in adjacent ion stages and move to shorter wavelengths with increasing ionization.

Spectral narrowing in mixed Δn=0 arrays

In spectra due to $4p^6 4d^{N+1}$- $4p^6 4d^N 4f$ + $4p^5 4d^{N+2}$ transitions

Configuration interaction causes

No CI

- Spectral narrowing.
- Strong peaking of oscillator strength.

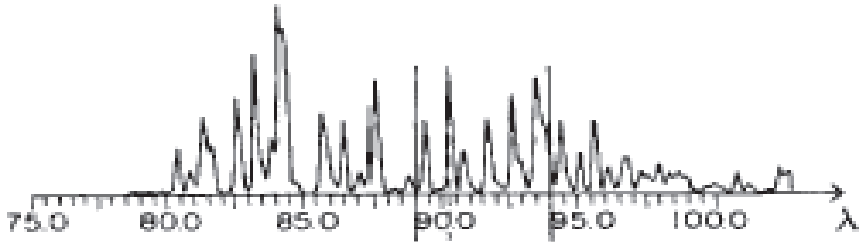

Pr XXII: $4p^6 4d^2$- $4p^6 4d4f$ + $4p^5 4d^3$

Localisation of transitions at ~ the same position in successive ion stages

CI

Centre of gravity of array

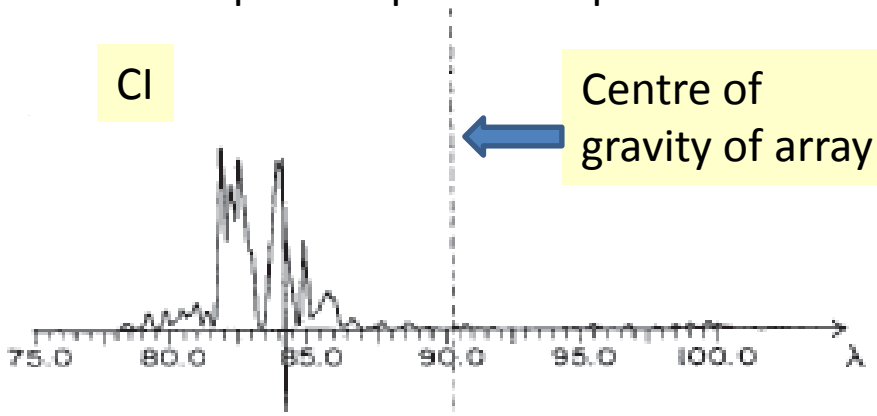

(Mandelbaum et al. Phys. Rev. A35, 5051, 1987)

CI effects (mixing) should diminish as Z increases

$4p^6 4d^{N+1} - 4p^6 4d^N 4f$

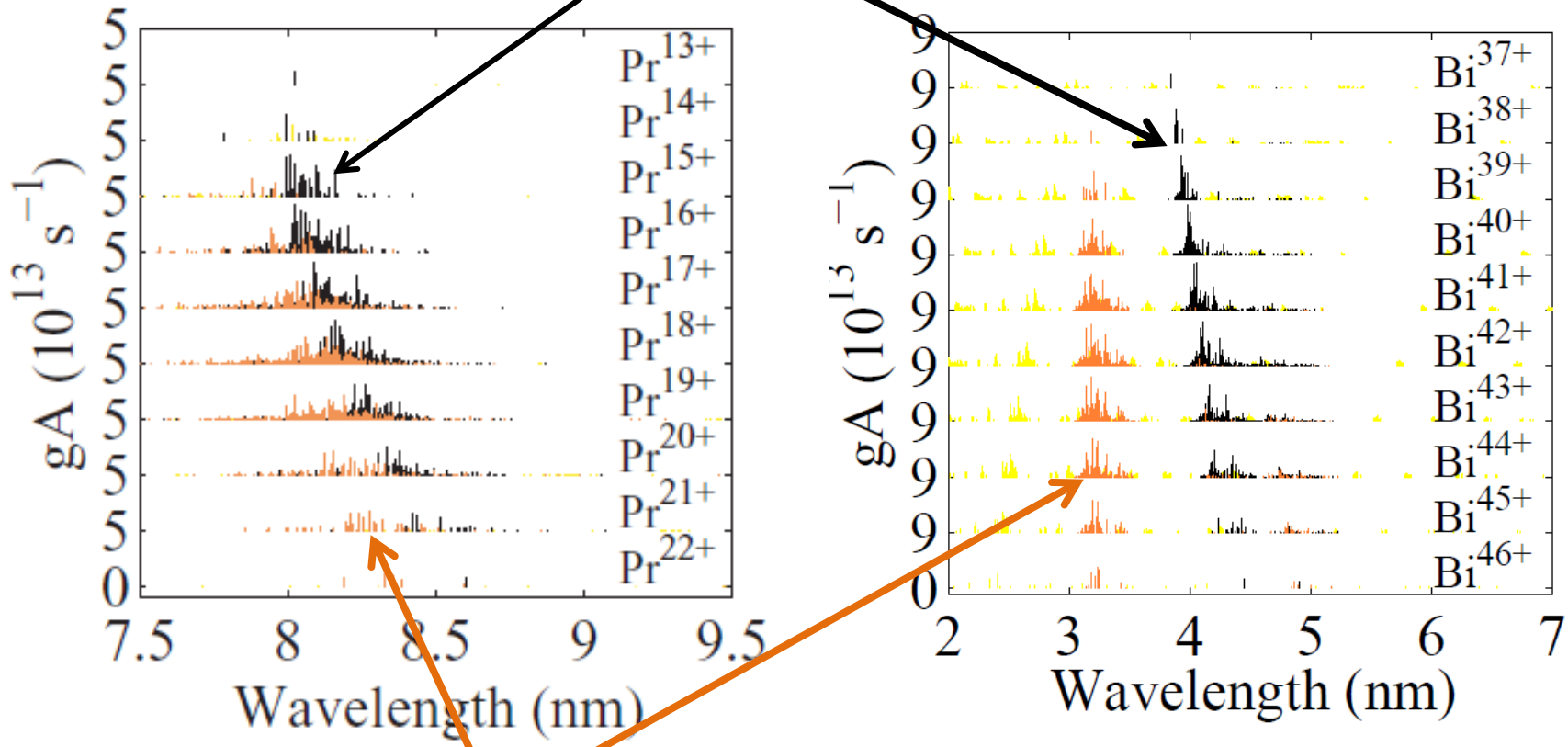

$4p^6 4d^{N+1} - 4p^5 4d^{N+2}$

Kilbane and O'Sullivan PRA 82, 062504 (2010)
Kilbane JPB 44 165006 (2011)

Evolution with Z of Δn=0, n=4 – n=4 UTAs

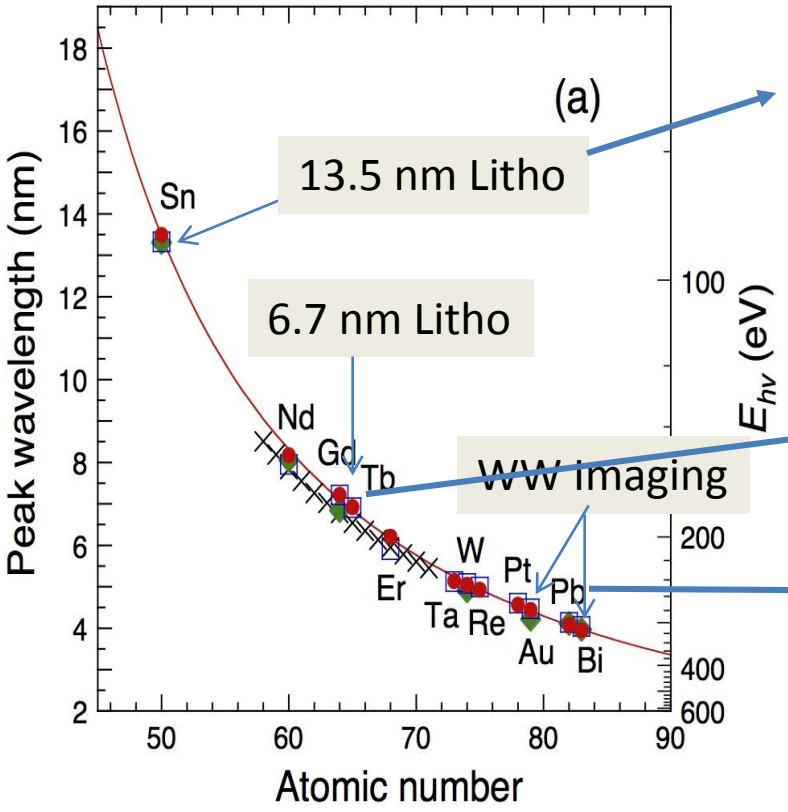

13.5 nm Litho

T_e~ 40eV

6.7 nm Litho

WW imaging

T_e>500 eV

Plasma electron temperature required increases with Z

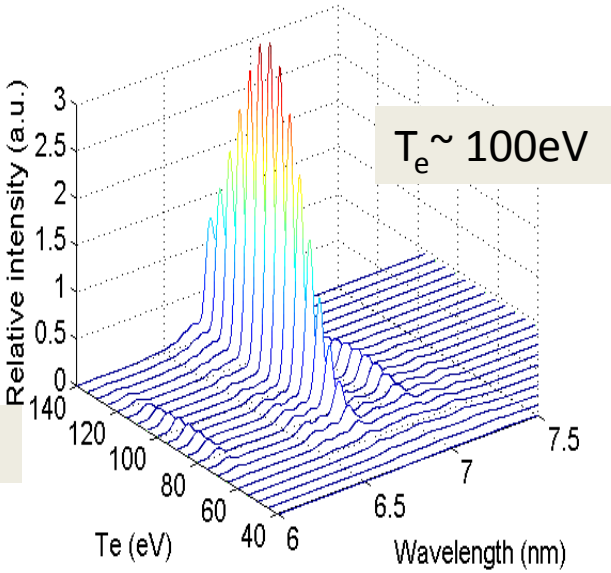

T_e~ 100eV

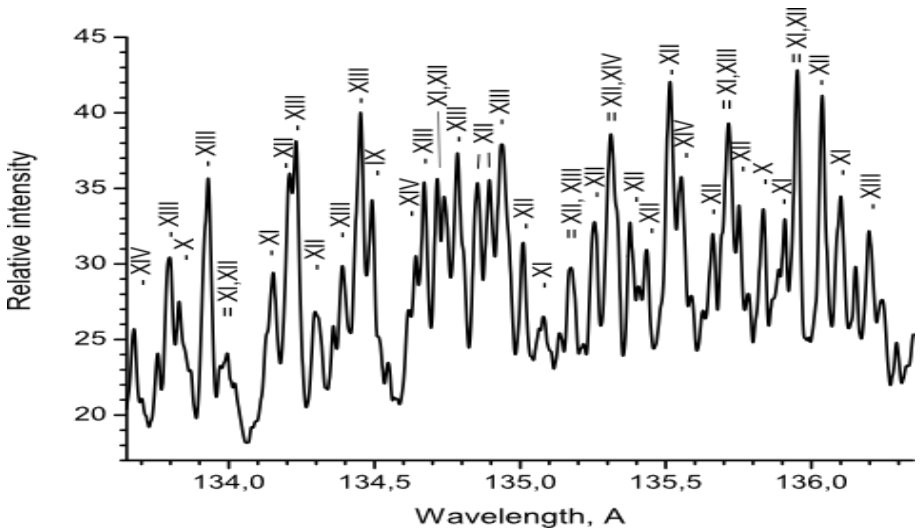

Analysis of Sn by Churilov and Ryabtsev
Phys. Scr. 73 614-619, 2006

Complexity of Δn=0 transitions in Pt XXXIV ($4d^9$) to Pt XLII ($4d^1$)

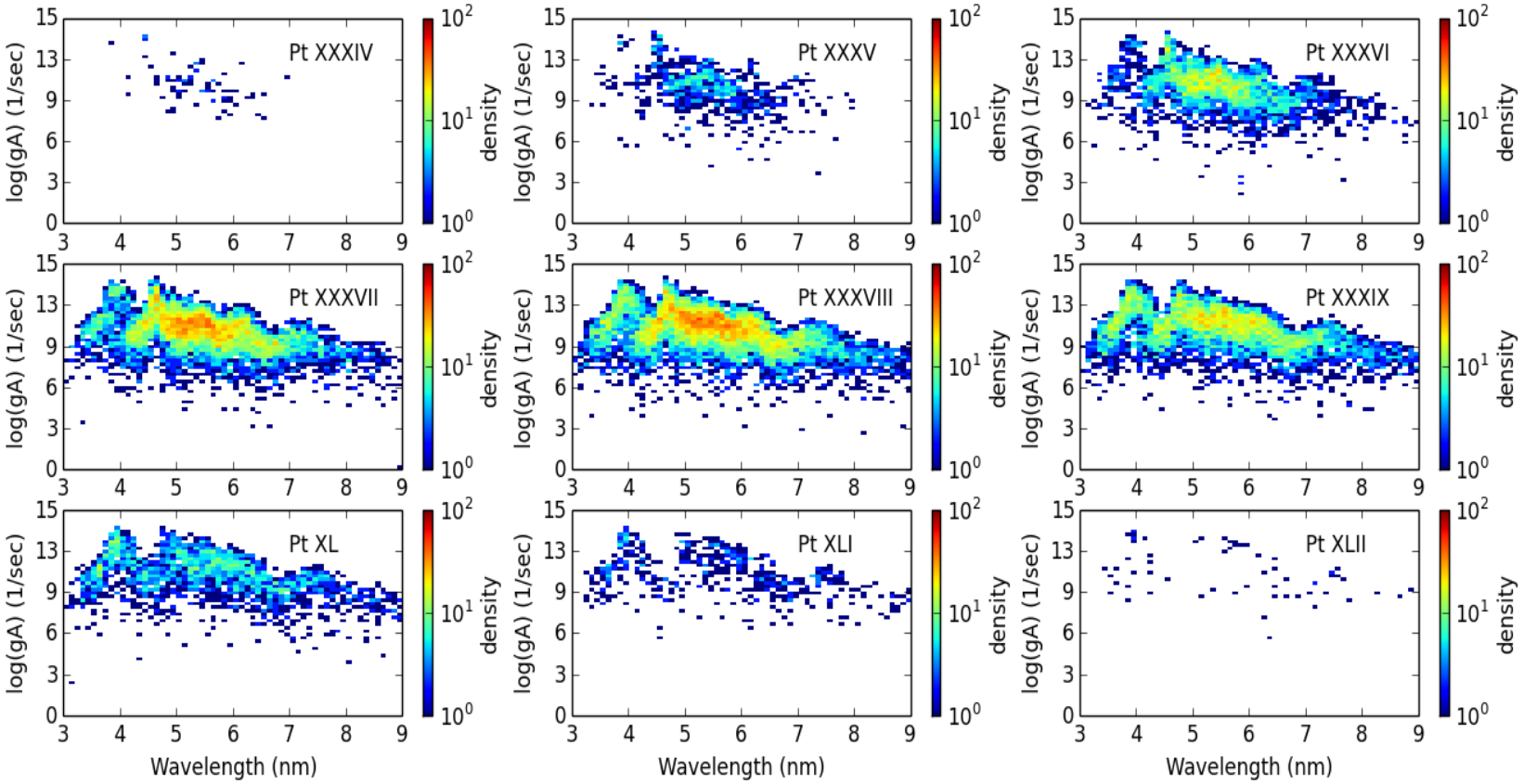

$4p^6 4d^m - 4p^5 4d^{m+1} + 4p^6 4d^{m-1} 4f$ transitions

Additional complexity at higher Z, $4d^{10}4f^{N}$- $4d^{9}4f^{N+1}$ Arrays: Pt XX, (N=13)- Pt XXXIII, (N=0)

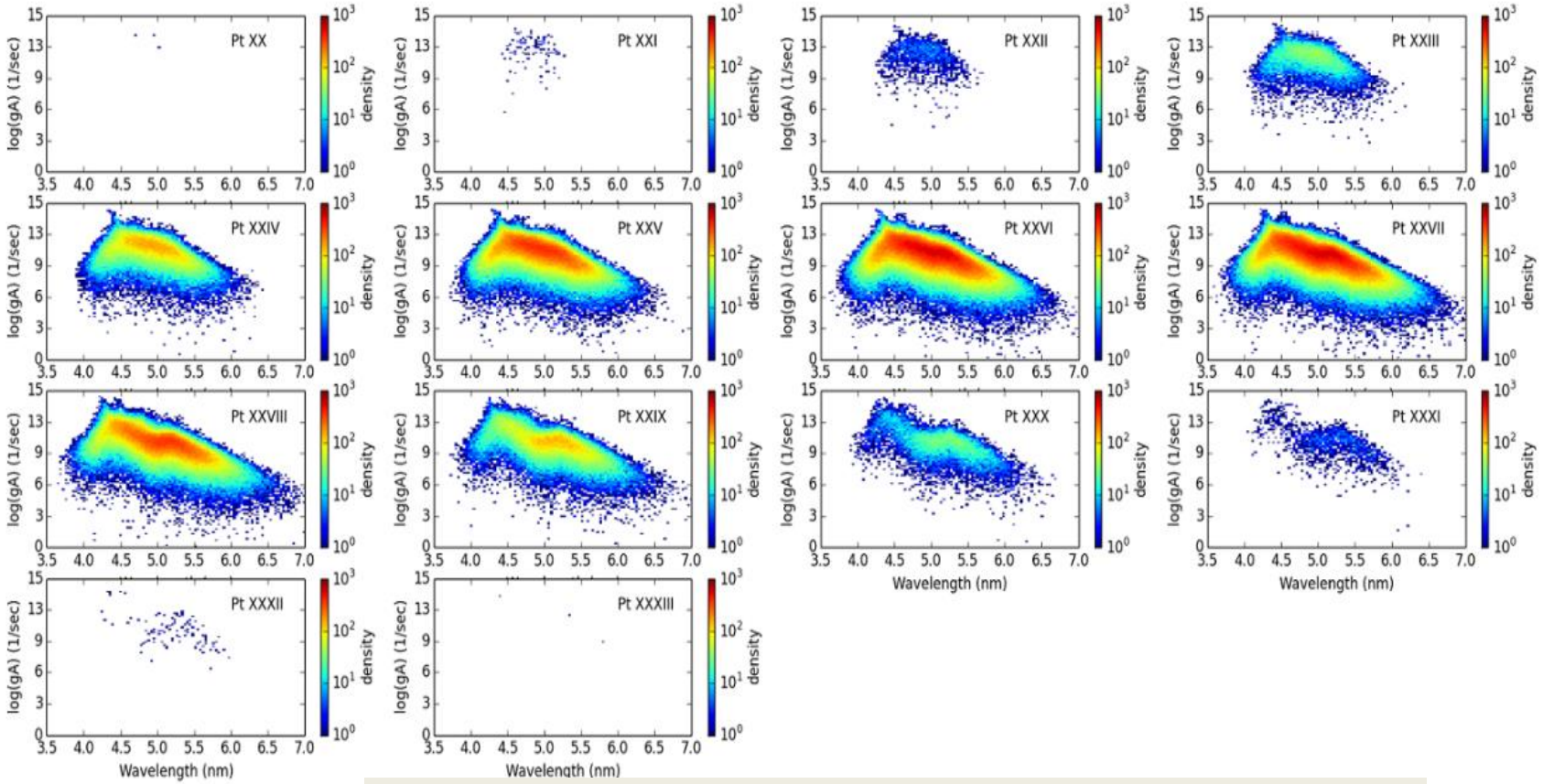

The most important transitions occur in Ag-like, Pd-like and Rh-Like Ions with $4d^{10}4f$, $4d^{10}$ and $4d^{9}$ ground states

(Sugar and Kaufman Phys. Scr. ***24,*** *742 (1982) and* ***26****, 417 (1984)*

Δn = 0 4-4 UTAs in the water window region, Au, Pb and Bi

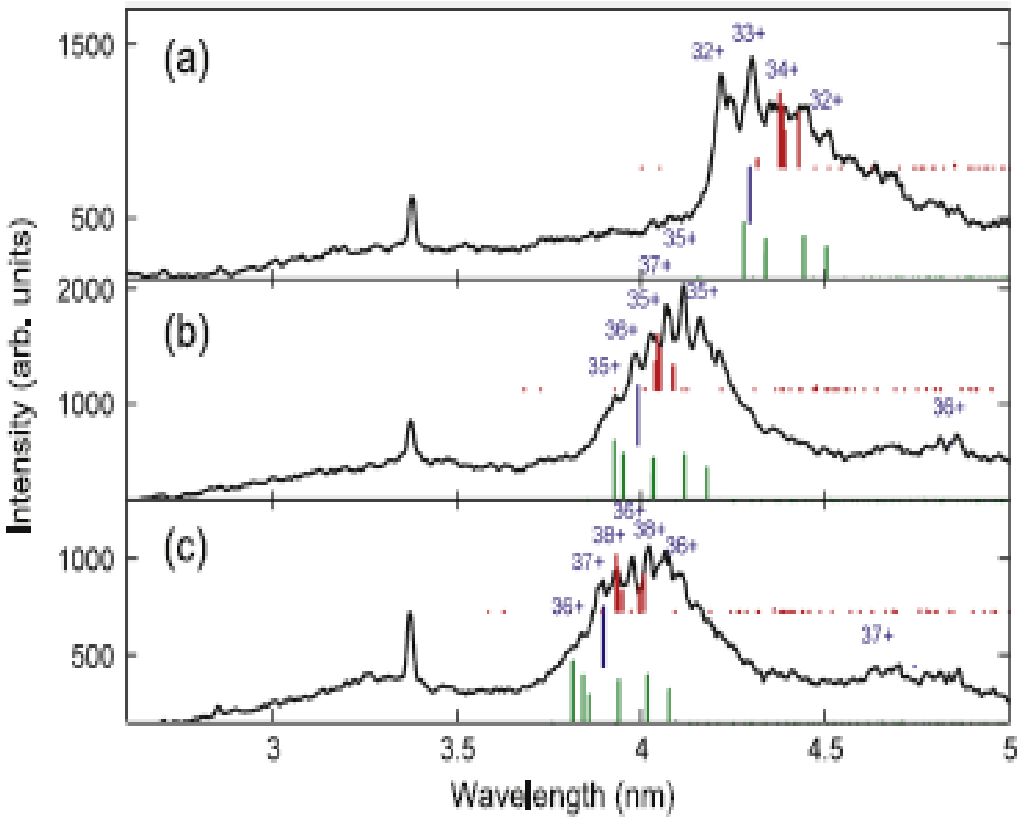

- Au, Pb and Bi injected using LPP or pellet.
- Spectra dominated by resonant line emission to the ground state
- Only Ag-, Pd- and Rh-like ions give line emission
- Absorption free

Δn = 0 4-4 UTAs in a Bi LPP; comparison with calculations

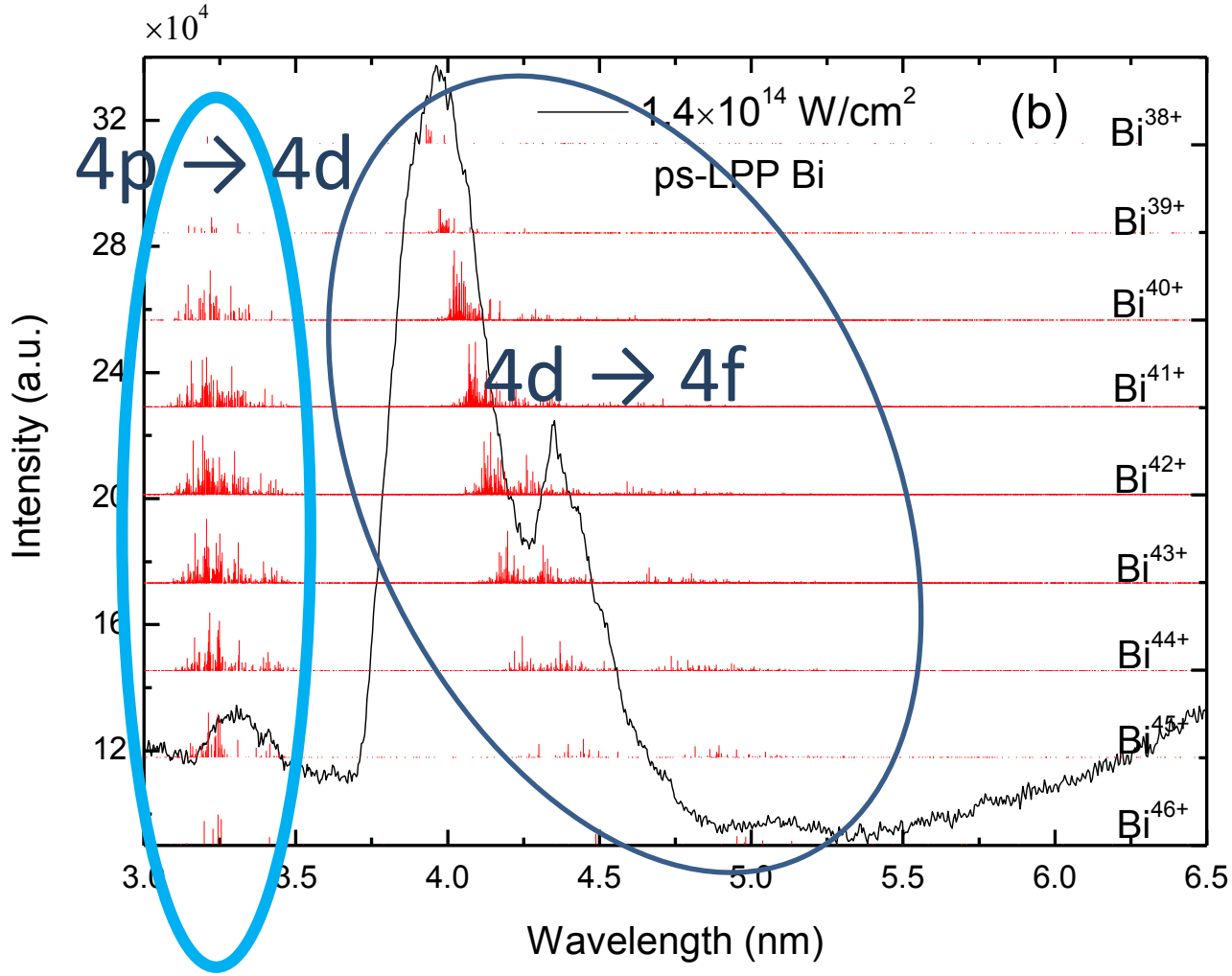

4p → 4d involve creation of a hole in sub-valence 4p subshell, not strong in emission. More important for absorption. Same probably true for strongesr $4d^{10}4f^{N}$-$4d^{9}4f^{N+1}$ lines

Complexity of Δn=0 transitions in Bi XXXIX ($4d^9$)- Bi XLVII ($4d^1$)

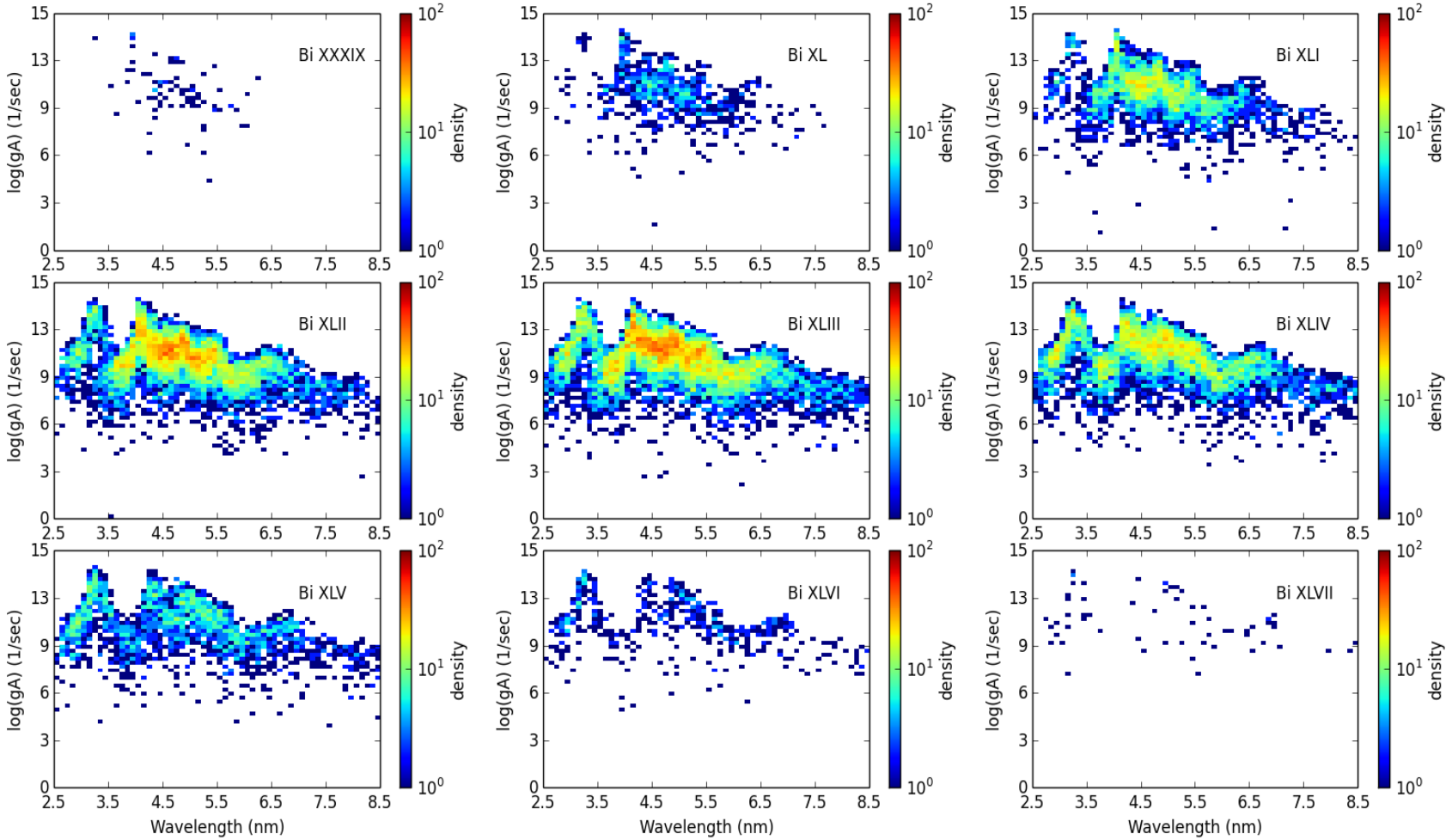

$4p^64d^m$-$4p^54d^{m+1}$+$4p^64d^{m-1}4f$ transitions

Δn = 1 UTAs

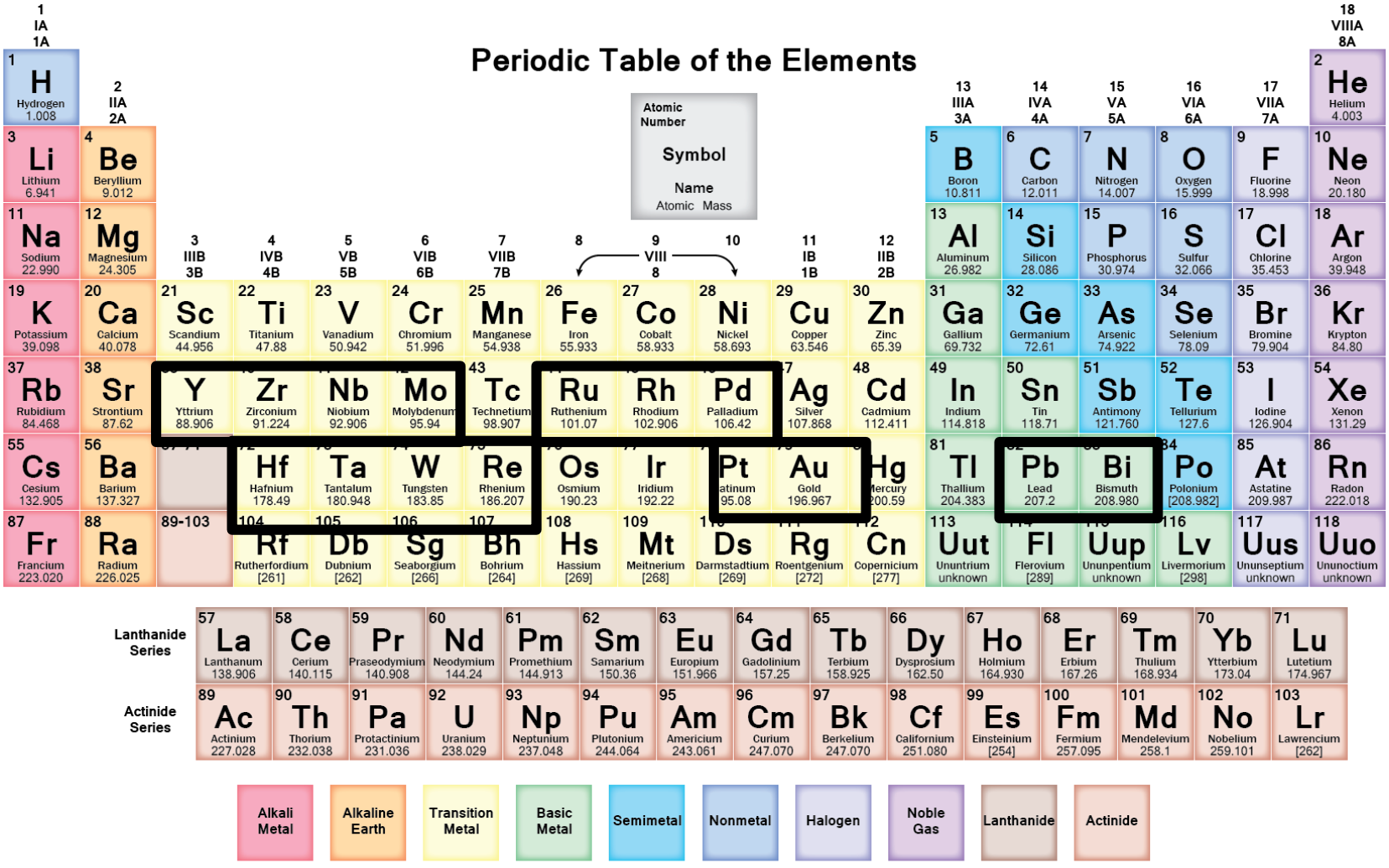
Periodic Table of the Elements
Atomic Number
Symbol
Name
Atomic Mass
1 IA 1A
2 IIA 2A
3 IIIB 3B
4 IVB 4B
5 VB 5B
6 VIB 6B
7 VIIB 7B
8
9 VIII 8
10
11 IB 1B
12 IIB 2B
13 IIIA 3A
14 IVA 4A
15 VA 5A
16 VIA 6A
17 VIIA 7A
18 VIIIA 8A
1 H Hydrogen 1.008
2 He Helium 4.003
3 Li Lithium 6.941
4 Be Beryllium 9.012
5 B Boron 10.811
6 C Carbon 12.011
7 N Nitrogen 14.007
8 O Oxygen 15.999
9 F Fluorine 18.998
10 Ne Neon 20.180
11 Na Sodium 22.990
12 Mg Magnesium 24.305
13 Al Aluminum 26.982
14 Si Silicon 28.086
15 P Phosphorus 30.974
16 S Sulfur 32.066
17 Cl Chlorine 35.453
18 Ar Argon 39.948
19 K Potassium 39.098
20 Ca Calcium 40.078
21 Sc Scandium 44.956
22 Ti Titanium 47.88
23 V Vanadium 50.942
24 Cr Chromium 51.996
25 Mn Manganese 54.938
26 Fe Iron 55.933
27 Co Cobalt 58.933
28 Ni Nickel 58.693
29 Cu Copper 63.546
30 Zn Zinc 65.39
31 Ga Gallium 69.732
32 Ge Germanium 72.61
33 As Arsenic 74.922
34 Se Selenium 78.09
35 Br Bromine 79.904
36 Kr Krypton 84.80
37 Rb Rubidium 84.468
38 Sr Strontium 87.62
39 Y Yttrium 88.906
40 Zr Zirconium 91.224
41 Nb Niobium 92.906
42 Mo Molybdenum 95.94
43 Tc Technetium 98.907
44 Ru Ruthenium 101.07
45 Rh Rhodium 102.906
46 Pd Palladium 106.42
47 Ag Silver 107.868
48 Cd Cadmium 112.411
49 In Indium 114.818
50 Sn Tin 118.71
51 Sb Antimony 121.760
52 Te Tellurium 127.6
53 I Iodine 126.904
54 Xe Xenon 131.29
55 Cs Cesium 132.905
56 Ba Barium 137.327
72 Hf Hafnium 178.49
73 Ta Tantalum 180.948
74 W Tungsten 183.85
75 Re Rhenium 186.207
76 Os Osmium 190.23
77 Ir Iridium 192.22
78 Pt Platinum 195.08
79 Au Gold 196.967
80 Hg Mercury 200.59
81 Tl Thallium 204.383
82 Pb Lead 207.2
83 Bi Bismuth 208.980
84 Po Polonium [208.982]
85 At Astatine 209.987
86 Rn Radon 222.018
87 Fr Francium 223.020
88 Ra Radium 226.025
89-103
104 Rf Rutherfordium [261]
105 Db Dubnium [262]
106 Sg Seaborgium [266]
107 Bh Bohrium [264]
108 Hs Hassium [269]
109 Mt Meitnerium [268]
110 Ds Darmstadtium [269]
111 Rg Roentgenium [272]
112 Cn Copernicium [277]
113 Uut Ununtrium unknown
114 Fl Flerovium [289]
115 Uup Ununpentium unknown
116 Lv Livermorium [298]
117 Uus Ununseptium unknown
118 Uuo Ununoctium unknown
Lanthanide Series
57 La Lanthanum 138.906
58 Ce Cerium 140.115
59 Pr Praseodymium 140.908
60 Nd Neodymium 144.24
61 Pm Promethium 144.913
62 Sm Samarium 150.36
63 Eu Europium 151.966
64 Gd Gadolinium 157.25
65 Tb Terbium 158.925
66 Dy Dysprosium 162.50
67 Ho Holmium 164.930
68 Er Erbium 167.26
69 Tm Thulium 168.934
70 Yb Ytterbium 173.04
71 Lu Lutetium 174.967
Actinide Series
89 Ac Actinium 227.028
90 Th Thorium 232.038
91 Pa Protactinium 231.036
92 U Uranium 238.029
93 Np Neptunium 237.048
94 Pu Plutonium 244.064
95 Am Americium 243.061
96 Cm Curium 247.070
97 Bk Berkelium 247.070
98 Cf Californium 251.080
99 Es Einsteinium [254]
100 Fm Fermium 257.095
101 Md Mendelevium 258.1
102 No Nobelium 259.101
103 Lr Lawrencium [262]
Alkali Metal
Alkaline Earth
Transition Metal
Basic Metal
Semimetal
Nonmetal
Halogen
Noble Gas
Lanthanide
Actinide
© 2014 Todd Helmenstine
sciencenotes.org

Δn=1 transitions in 2nd transition row

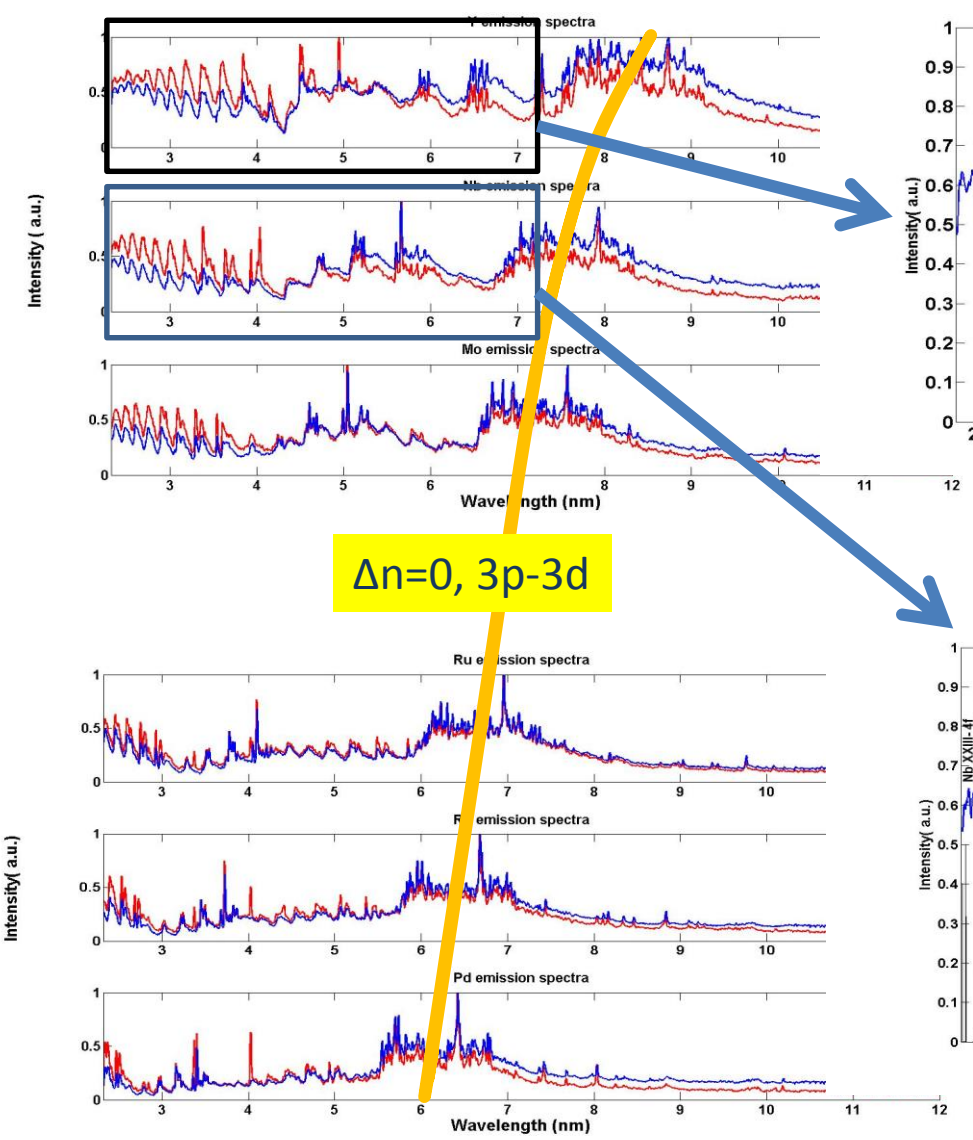

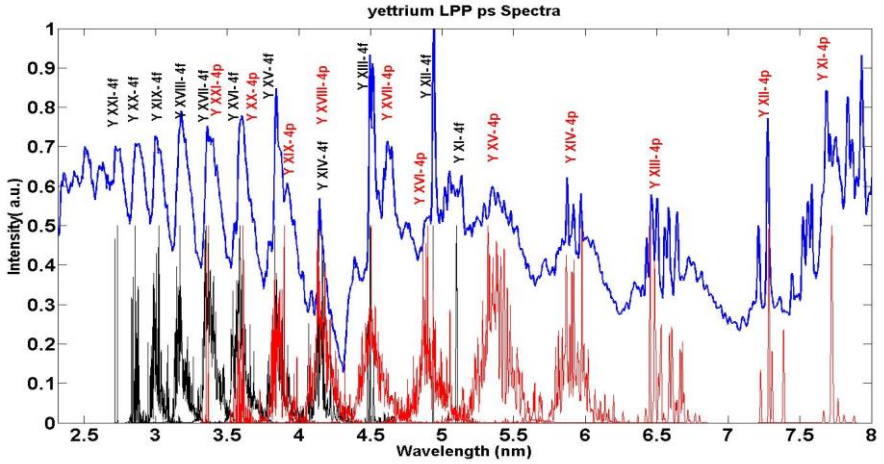

Δn=1, 3d-4p and 3d-4f

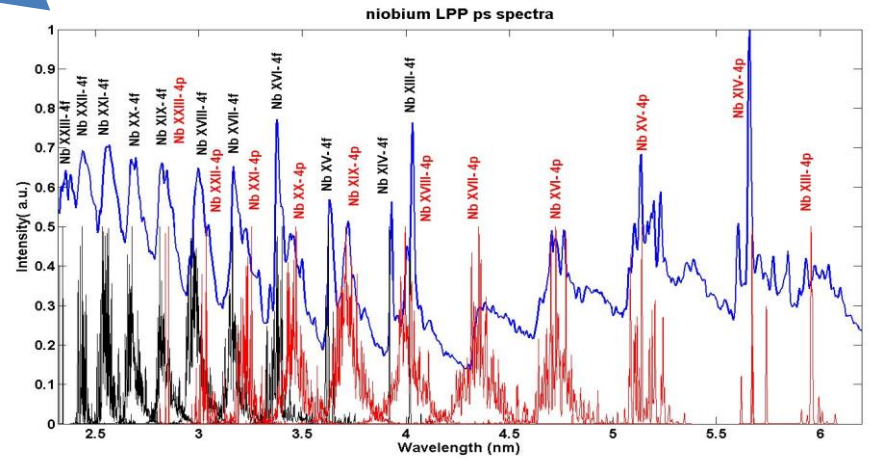

Importance of satellite line emission

Satellite line emission of type $3d^{n-1}4s$-$3d^{n-2}4s4f$ very important.

Comparison between the observed spectrum and numerically calculated spectra of Zr with and without satellite lines assuming a steady-state CR model for different plasma temperatures of 100 (a), 150 (b), and 200 eV (c).

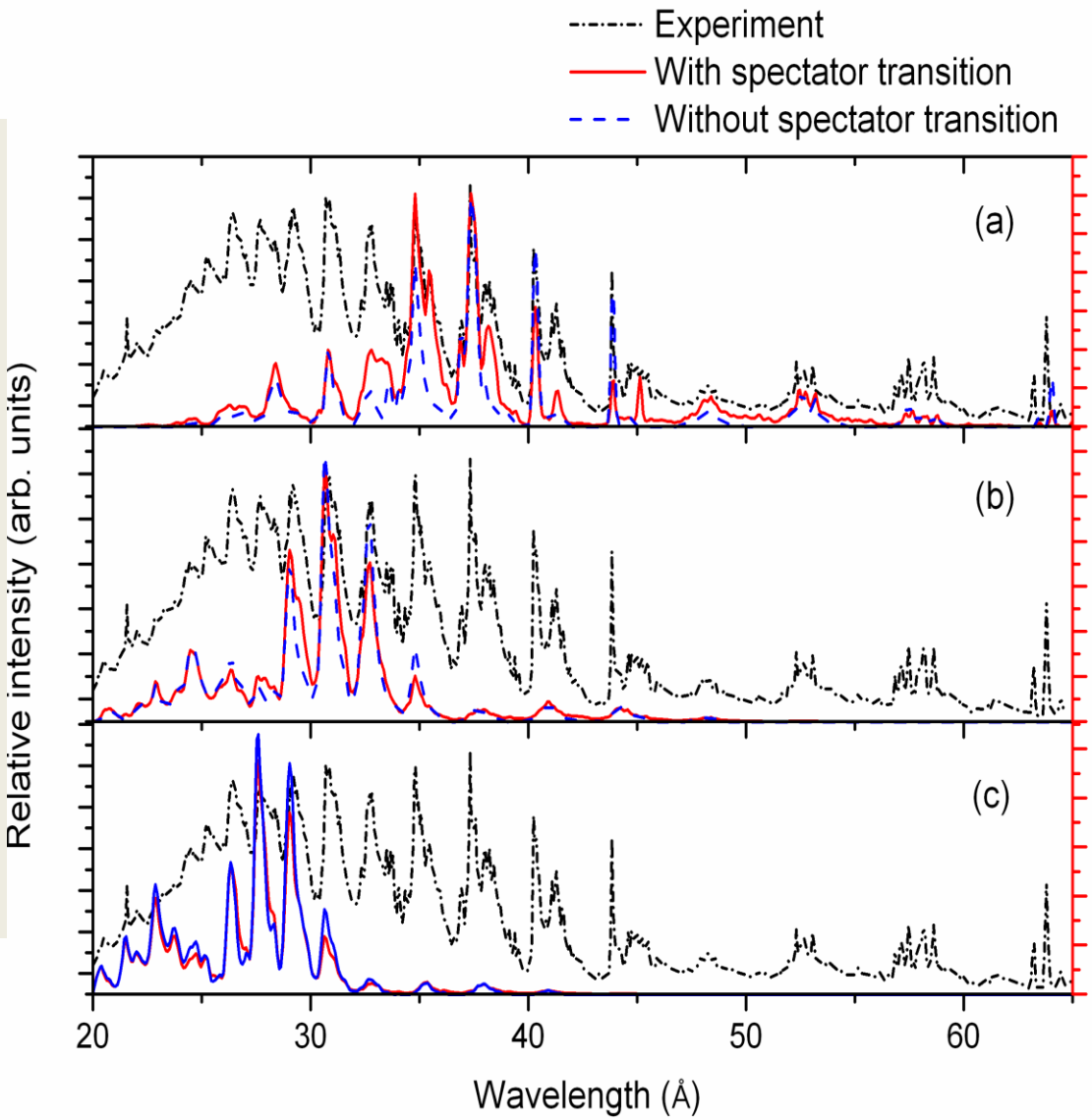

Mo as a WW source: CE vs pulse energy or Φ @ different λ

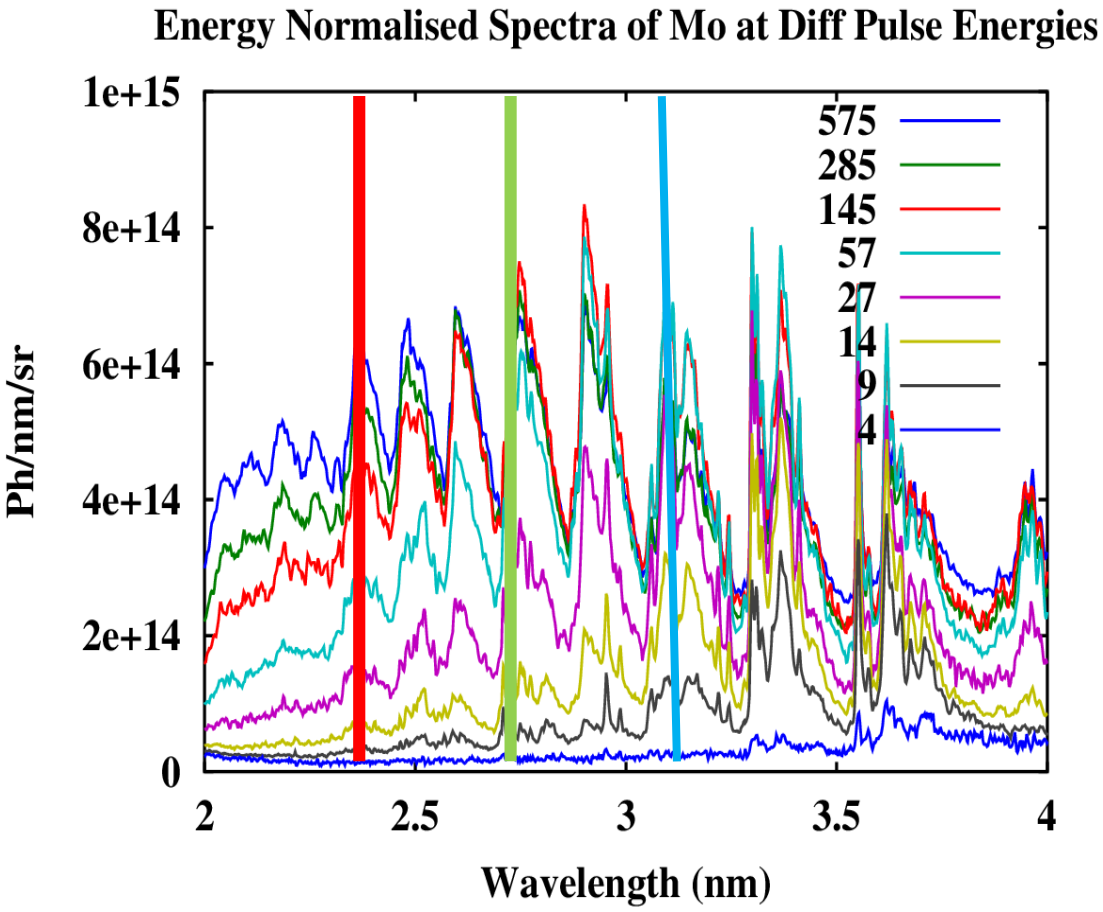

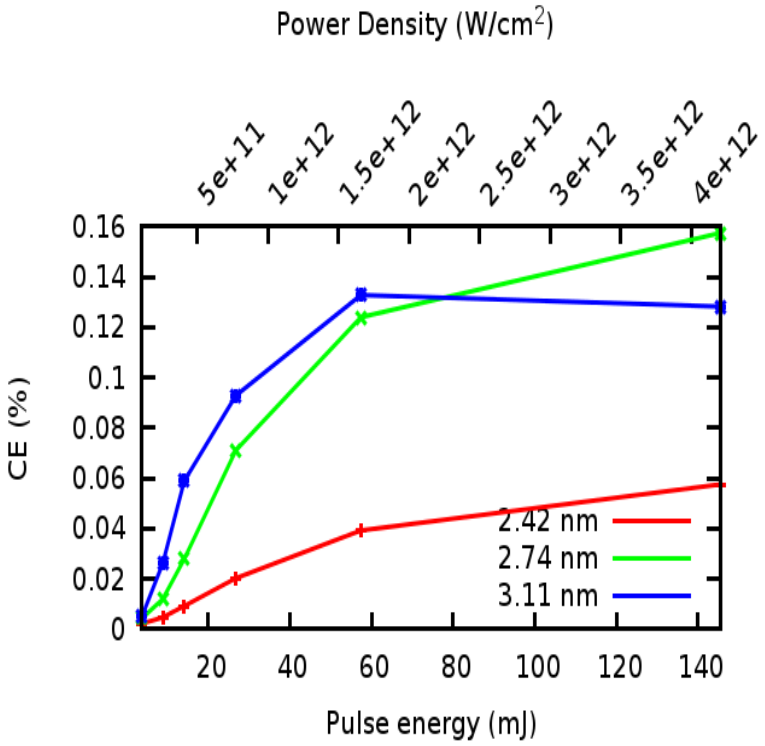

3rd transition row spectra

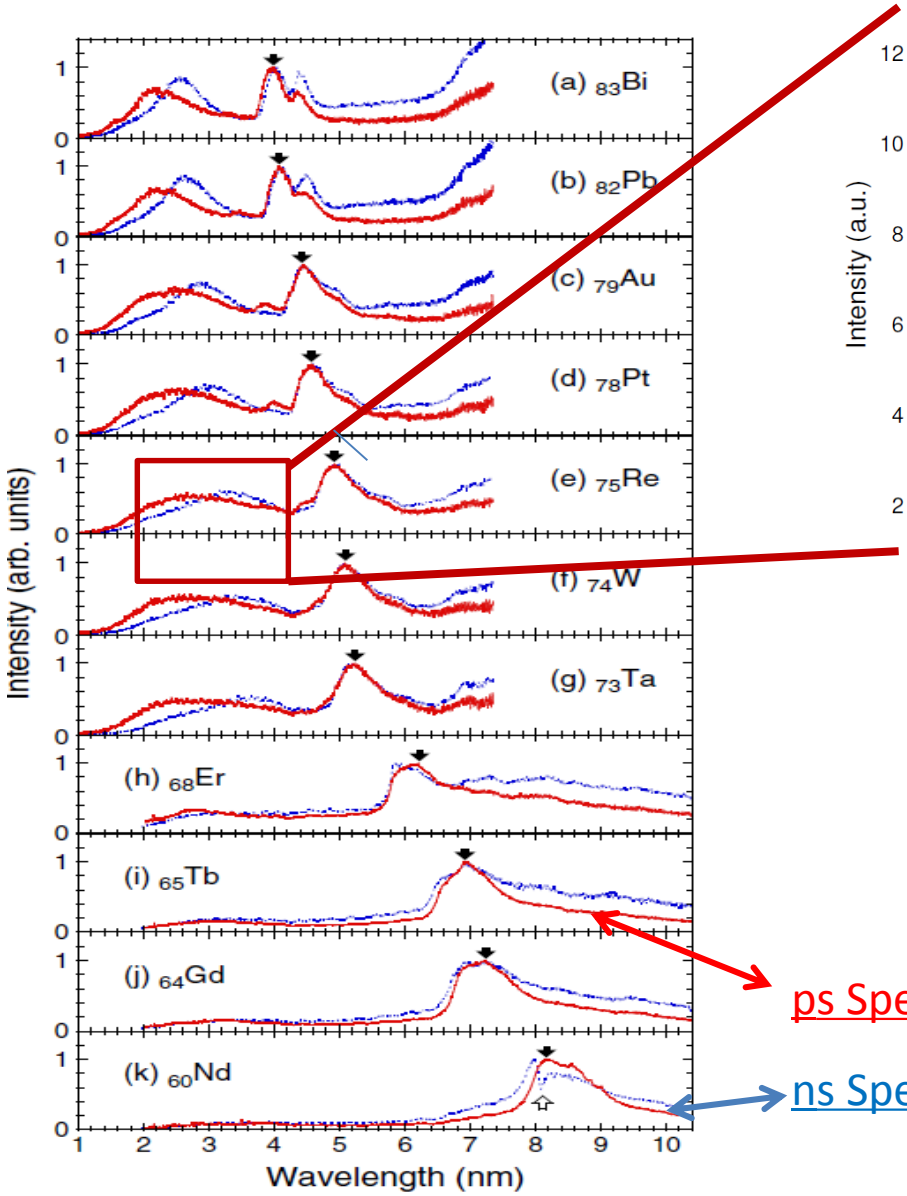

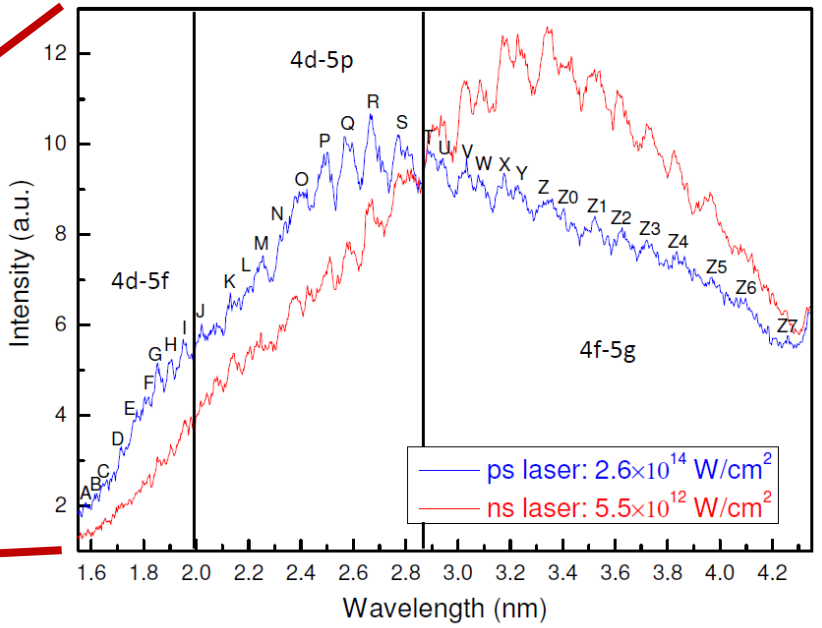

ps Spectra

ns Spectra

Spectrum of Re for Nd:YAG LPPs with 7 ns and 170 ps (b) laser pulse durations

Spectra dominated by 4-5 UTAs at shorter λ

Spectral identification in Re (Z=75)

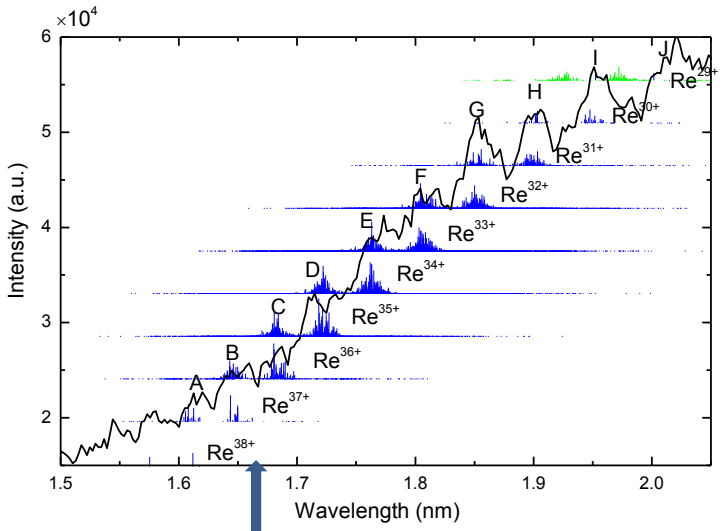

$4d^N$-$4d^{N-1}5p$ in Re^{29+}-Re^{38+} and $4d^{N-1}5s^1$-$4d^{N-2}5s^15p$ satellites in Re^{29+}

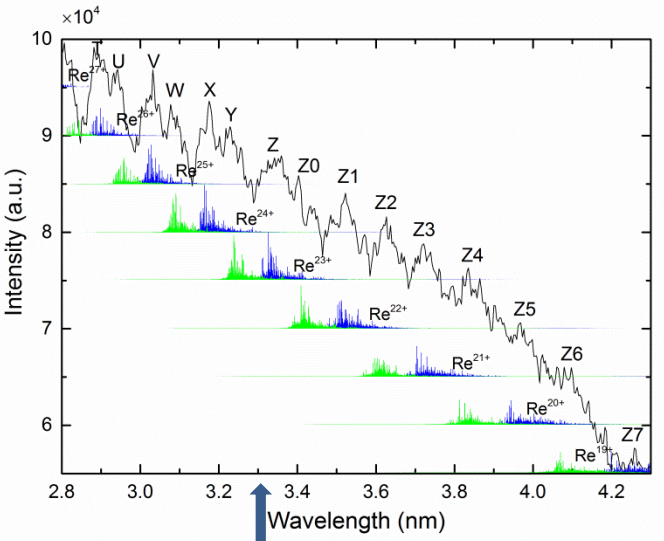

$4d^N$-$4d^{N-1}5f$ in Re^{29+}-Re^{38+} and $4d^{N-1}5s^1$-$4d^{N-2}5s^15f$ satellites in Re^{29+}

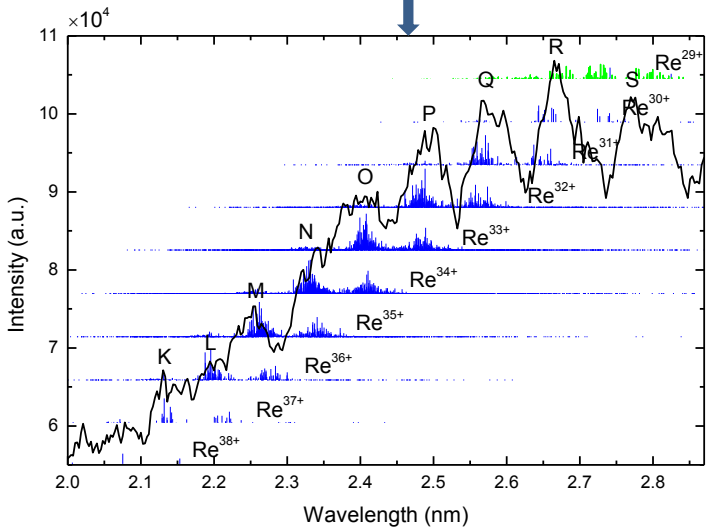

$4f^N$-$4f^{N-1}5g$ in Re^{21+}-Re^{27+} and $4f^{N-1}5s$-$4f^{N-2}5s^15g$ satellites in Re^{19+}-Re^{27+}

SXR spectra of Pt (Z=78)

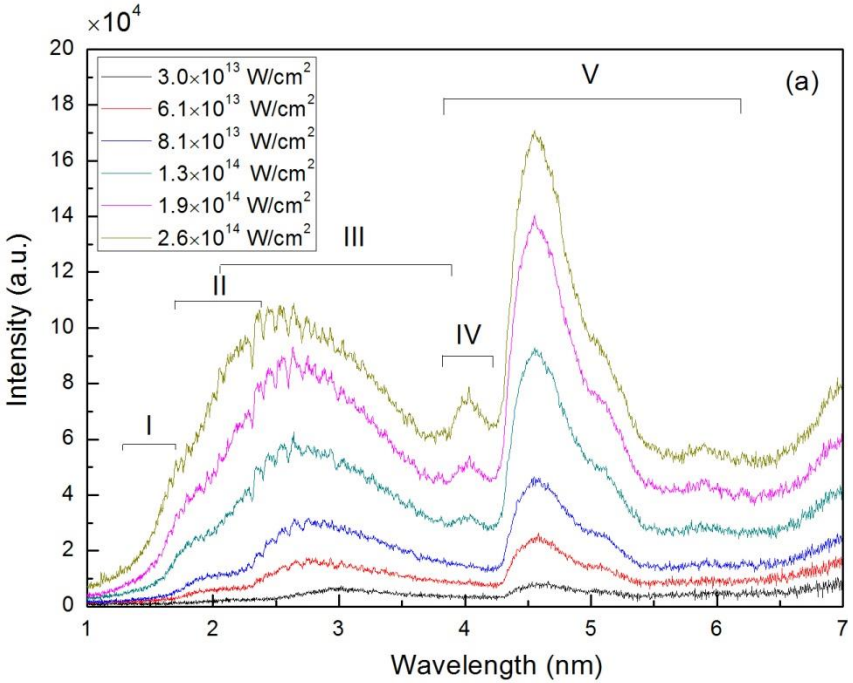

LPP produced by 170 ps Nd:YAG laser

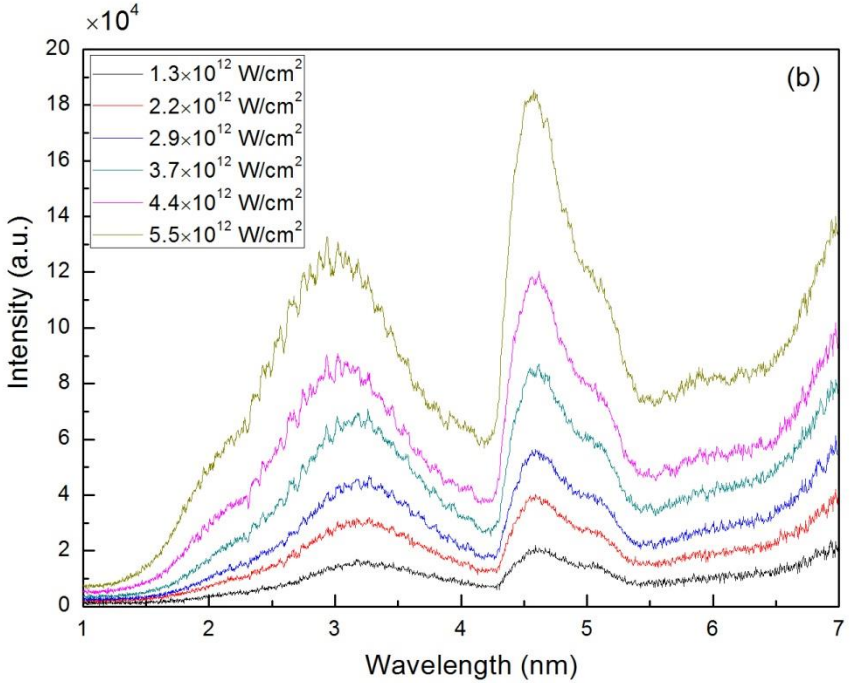

LPP produced by 10 ns Nd:YAG laser

The contributions from different transitions are labelled as follows: (I) $\Delta n=1$, $4d^m$-$4d^{m-1}5f$; (II) $\Delta n=1$, $4d^m$-$4d^{m-1}5p$; (III) $\Delta n=1$, $4f^m$-$4f^{m-1}5g$ and $4f^{m-1}5l$-$4f^{m-2}5l5g$ (l=s, p); (IV) $\Delta n=0$, $4p^64d^m$-$4p^54d^{m+1}$; (V) $\Delta n=0$, $4p^64d^m$-$4p^54d^{m+1}$+$4p^64d^{m-1}4f$ and $4d^{10}4f^m$-$4d^94f^{m+1}$. (b) Pt spectra from ns-LPP recorded in the wavelength region 1-7 nm at six different power densities.

Δn=1, 4f-5g Transitions in Pt

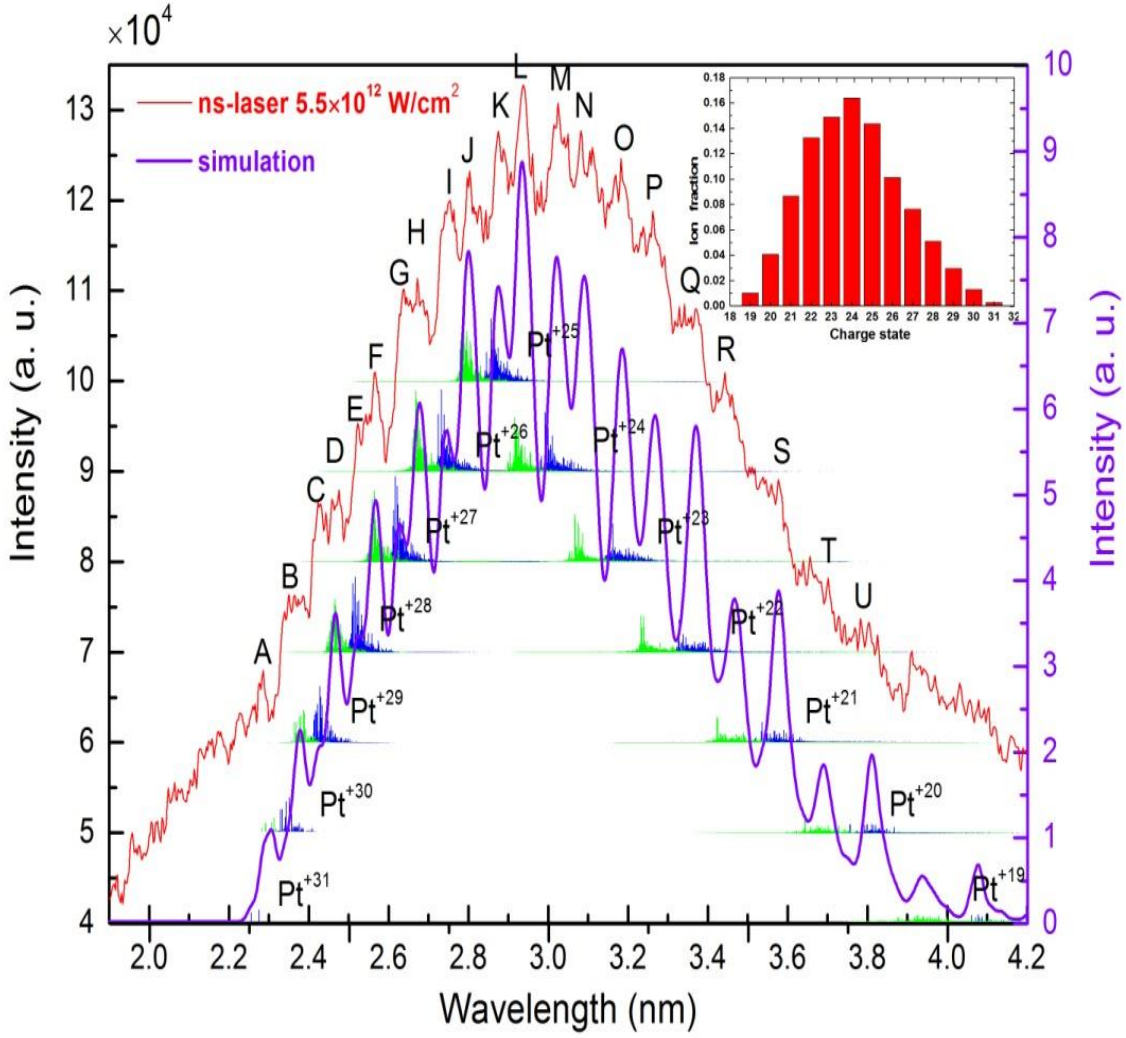

Comparison of calculated gA value distributions of $4d^{10}4f^{m}$-$4d^{10}4f^{m-1}5g$ and $4d^{10}4f^{m-1}5s$-$4d^{10}4f^{m-2}5s5g$ transitions in Pt XX-Pt XXXII and a simulated UTA spectrum with a measured Pt spectrum from a Nd:YAG ns-LPP.

The insert shows the ionic populations that fit the spectrum. The theoretical spectra are calculated gA-value distributions.

Plans /Conclusions

- Population information especially from calibrated ps spectra.
- Complete studies of high Z spectra. In particular, 4f-5g transitions in lanthanides and explore 4f,5p and 4f, 5s level crossing effects on the spectral appearance.
- Study emission from short pulse CO_2 plasmas, effects of prepulses.
- Δn=1 UTA in many elements can be found to match MLM reflectivity peaks. Build up comprehensive overview.
- Implement source in XUV microscope.

Thanks to:

Takako Kato, Daiji Kato, Inumi Murakami, Hiroyuki A Sakaue, National Institute for Fusion Science, Toki

Noboru Yugami, Utsunomiya University

Takamitsu Otsuka, Osaka University

Hajime Tanuma, Tokyo Metropolitan University,

Noboyuki Nakamura, Tokyo Electrocommunications University

Akira Endo and Jiri Lampouch, HiLase and Czech Technical University

John Costello, Dublin City University

Isaak Tobin, Tony Donnelly and James Lunney, Trinity College Dublin

Dong Chenzhong and Su Maogen, NWNU Lanzhou

Yuri Ralchenko and John Gillaspy, NIST, MD USA.

Larissa Juschkin, RWTH Aachen

Katsunobu Nishihara, Hiroaki Nishimura, Shinsuke Fujioka, ILE Osaka.

Science Foundation Ireland Principal Investigator Grant 07/IN1/I1771

EACEA Erasmus Mundus Project
EXTATIC framework partnership agreement FPA-2012-0033

Science Foundation Ireland International strategic collaboration award 13/ISCA/2846

JSPS, Japan Society for the promotion of Science KAKENHI grant 15H03759

Chinese Scholarship Council

National Natural Science Foundation of China, grant 11304235

Scientific Research Foundation of Hubei Province grant Q20131512

THANK YOU!